SAN096-3031C

CONF-9705120--1

Variation of High-Power Aluminum-Wire Array Z-Pinch Dynamics with Wire Number, Array Radius, and Load Mass

T. W. L. Sanford, R. C. Mock, B. M. Marder, T. J. Nash, and R. B. Spielman
Sandia National Laboratories, Albuquerque, NM 87185

D. L. Peterson and N. F. Roderick
Los Alamos National Laboratory, Las Alamos, NM 87545

J. H. Hammer and J. S. De Groot
Lawrence Livermore National Laboratory, Livermore, CA 94550

D. Mosher
Naval Research Laboratory, Pulsed Power Physics Branch, Washington, DC 20375

K. G. Whitney and J. P. Apruzese
Naval Research Laboratory, Radiation Hydrodynamics Branch, Washington, DC 20375

Abstract. A systematic study of annular aluminum-wire z-pinches on the Saturn accelerator shows that the quality of the implosion, including the radiated power, increases with wire number. Radiation magnetohydrodynamic (RMHC) xy simulations suggest that the implosion transitions from that of individual wire plasmas to that of a continuous plasma shell when the interwire spacing is reduced below ~ 1.4 mm. In the plasma-shell regime, the experimental implosions exhibit 1D- and 2D-code characteristics as evidenced by the presence of a strong first and a weak second radiation pulse that correlates with a strong and weak radial convergence. In this regime, many of the radiation and plasma characteristics are in agreement with those simulated by 2D-RMHC rz simulations. Moreover, measured changes in the radiation pulse width with variations in array mass and radius are consistent with the simulations and are explained by the development of 2D fluid motion in the rz plane. Associated variations in the K-shell yield are qualitatively explained by simple K-shell radiation scaling models.

INTRODUCTION

Increasing the azimuthal symmetry of cylindrical aluminum-wire arrays by significantly increasing wire number and decreasing the associated interwire spacing and wire size has resulted in the highest x-ray power (~ 40 TW) and narrowest x-ray pulse-width (~ 5 ns) measured for aluminum-wire implosions (1) on the 20-TW Saturn accelerator (2). At wire spacings of ~ 1.4 mm or less,

DISCLAIMER

radiation magnetohydrodynamic code (RMHC) (xy) simulations for Saturn predict that the implosion changes character from one of individual wire plasmas to that of a continuous plasma shell (1). In the plasma-shell regime, measurements and analyses show that as the wire number increases further, the quality of the implosion and the radiated power increase monotonically. Similar effects are found for tungsten wire implosions as discussed in Refs. 3 and 4 and papers at this conference.

Prior to these experiments, wire-array loads had been optimized for x-ray energy and power output only in the small-wire-number ($N \leq 40$) wire-plasma regime [5-7], where the array is now predicted (1) to implode inward as a set of discrete wire plasmas. The substantial improvement in implosion quality and associated radiated power that occurs in the plasma-shell regime (1) suggested that a reexamination of the radius and mass conditions that maximized the radiation output would be instructive. The more nearly 2D, azimuthally-symmetric nature of plasma-shell-implosion measurements could then be more realistically compared with rz RMHC simulations to gain insight into the fundamental physical processes, free of the large azimuthal asymmetries and resulting instabilities that have limited previous detailed comparisons. Moreover, 1D-RMHC simulations that utilize detailed radiation models not feasible in the 2D codes are used to infer the measured plasma conditions from the measured x-ray spectral data. Calculations done with either the multi-photon-group 2D Lagrangian code (L-RMHC) (8), which modeled 1 mm of the pinch length (9); the three-temperature 2D Eulerian code (E-RMHC) (10,11), which modeled the entire pinch length; or the detailed-multi-spectral 1D Lagrangian code (1D-RMHC) (12) are discussed here. Additionally, a need existed to assess the effect that longer implosion times would have on the pinch quality expected for the recently commissioned, 45-TW PBFA-Z accelerator [13,14]. For PBFA-Z, the optimal coupling of accelerator energy to the load was expected to occur for implosion times on the order of 100 ns, roughly twice that found for loads on the Saturn accelerator.

Accordingly, after the initial wire-number experimental series (1), two additional experimental series were conducted both to re-examine the conditions that optimize the XUV and K-shell x-ray output and to explore the longer-implosion-time regime using large-wire-number, plasma-shell-regime loads. In one series, the radius was held fixed, and the mass was varied (15). In the other series, the mass was held fixed near the mass that optimized the x-ray output, and the radius was varied (16). These two new experimental series enabled the K-shell-yield behavior to be measured in conjunction with the implosion quality over implosion durations of 40 to 90 ns.

A schematic of the generic arrangement used for all of the experiments and the equivalent-circuit model that was used as driver to the RMHC simulations is shown in Fig. 1. The particular arrangements and circuit model are discussed in detail elsewhere (1,9, and 17). In the initial wire-number scan, the array mass and radius were fixed at either ~ 0.62 mg and 8.56 mm or 0.84 mg and 12 mm for the 2-cm-long loads. The wire number was changed incrementally from 10 to 192 by varying the diameter of the individual wires from 37 to 10 μm, permitting interwire spacings from 6 to 0.4 mm to be explored. For the mass scan, the radius was fixed at 12 mm and the mass was varied between 0.42 and 3.36 mg by changing the diameter and the number of wires. For masses of 0.84 mg and greater, the number of wires was held at 192 (0.4 mm interwire spacing), and the wire diameter was varied between 10 and 20 μm in 2.54-μm steps. Because the smallest diameter aluminum wire available was 10 μm, the mass region below 0.84 mg was necessarily explored by reducing the number of wires, resulting in an increase in the interwire spacing to 0.8 mm. For the radius scan, the array mass was held fixed at 0.6 mg (136, 10.2-μm-diameter wires), where high powers had been produced in the mass scan. These arrays had interwire spacings that varied from 0.4 mm for the smallest array diameter to 0.94 mm for the largest array diameter.

In this paper, the results of the initial wire-number scan are reviewed. The plasma and radiation generated in the plasma-shell regime are then characterized and compared with the L-RMHC, E-RMHC, and 1D-RMHC simulations. Lastly, the variation of these plasma and radiation characteristics with mass and radius in the plasma-shell regime is discussed and contrasted with results produced by the E-RMHC.

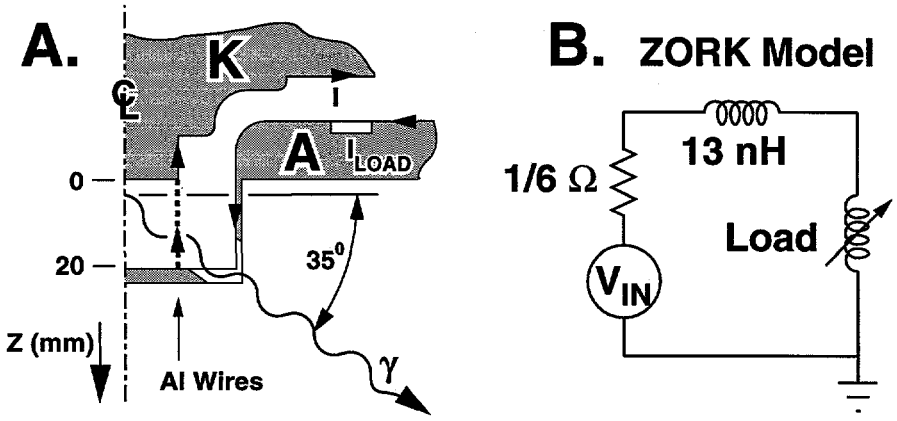

FIGURE 1. (A) Schematic of experimental arrangement showing (B) equivalent circuit. The 13-nh corresponds to the system inductance up to the initial wire location.

WIRE NUMBER VARIATION

The improvement in pinch quality with wire number in both geometries (R = 8.56 and 12 mm) is evident in three ways: (1) the x-ray pinhole camera images that show increased radial convergence (Fig. 2A) and associated total increased radiated energy (Fig. 2B), (2) the load-current traces that show an increased inductive current notch at peak compression, and (3) the x-ray pulses that show reduced radiation rise time and pulse width (Fig. 3), and the associated increased radiated power (Fig. 4). The increase in measured radiated energy is consistent, within a scale factor (1.3±0.2), with that expected from the increased kinetic-energy input predicted by the ZORK coupled circuit and slug-model code (18) (Fig. 2B), using the measured radial convergence from x-ray pinhole photographs (Fig. 2A). For high-wire-number loads, the current and main radiation pulse shapes are consistent with those simulated by the rz RMHCs (1,9,15,16).

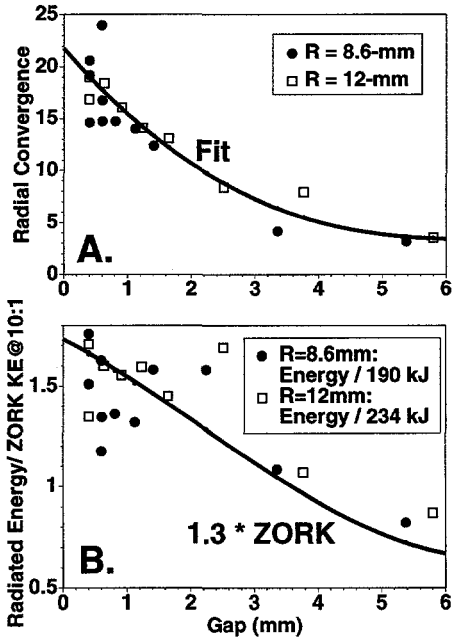

FIGURE 2. (A) Radial convergence determined from time-integrated pinhole images filtered to view x-rays greater than 1 keV versus interwire gap (g): Fit = 22 - 7.2 g + 0.9 g^2 - 0.0034 g^3. Comparison of (B) total radiated energy measured in bolometer (uncorrected for spectral response and viewing angle) normalized by calculated ZORK kinetic energy for a 10-to-1 radial convergence (190 and 234 kA for R = 8.6 and R = 12 mm, respectively) with that predicted by ZORK using measured radial convergence of Fig. 2A.

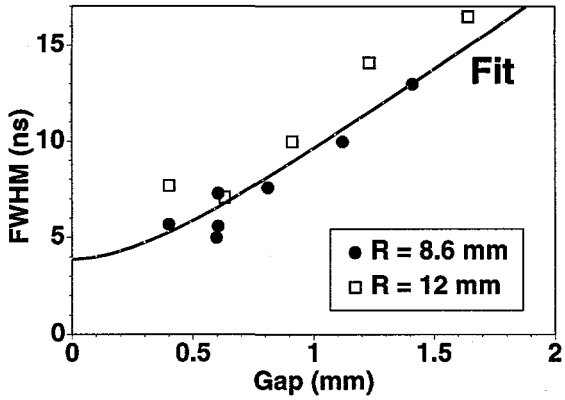

FIGURE 3. Estimated total-radiated--power pulse width (measured in XRD filtered by 1-μm Kimfol) versus interwire gap (g). Fit = $\sqrt{(3.9\pm2)^2+[(8.8\pm2)g]^2}$.

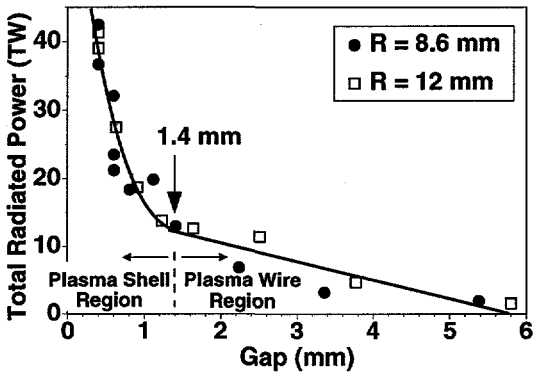

FIGURE 4. Total radiated power measured by bolometer (corrected for pulse shape distortion, spectral response, and viewing angle) versus interwire gap.

Plotting data against the interwire gap (as exemplified in Figs. 2-4) for the two geometries yields single curves, dependent on spacing alone. The dramatic increase in power below a spacing of ~ 1.4 mm is associated with the calculated transition between the implosion of individual wire plasmas (Fig. 5A) and that of a continuous plasma shell (Fig. 5B) (1). In the plasma-shell regime (i.e., gap < 1.4 mm), the improvement in pinch quality and radiation output with decreasing spacing is associated with a calculated increase in the merger of the wire plasmas prior to the implosion of the array.

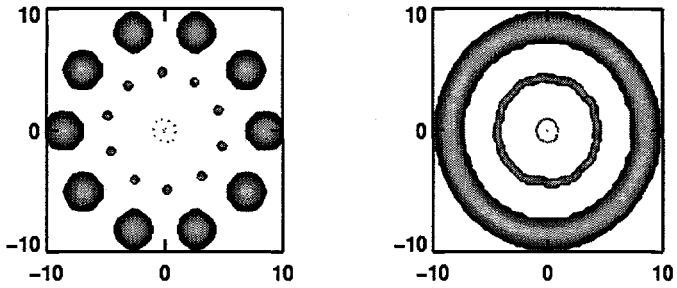

FIGURE 5. xy-RMHC simulations for (A) 10- and (B) 40-wire 8.6-mm implosions at 86, 11, 3, and 0 ns before stagnation. Azimulthal orientations at different times are not correlated.

PLASMA-SHELL REGIME CHARACTERISTICS

Loads in the plasma-shell regime, having interwire spacings of less than ~ 0.6 mm, exhibit both a strong first and weaker second radiation pulse (Fig. 6A) that correlates in time with strong and weaker measured radial convergences (Fig. 6B). The radial convergence is obtained from radial lineouts of time-resolved x-ray images such as those shown in Fig. 7 for Shot 2235 (m = 1.3 mg, R = 12 mm, N = 192 wires) taken during the mass scan, or in Fig. 8 for Shot 2085 (m = 0.6 mg, R = 8.6 mm, N = 90 wires), taken during the wire-number scan.

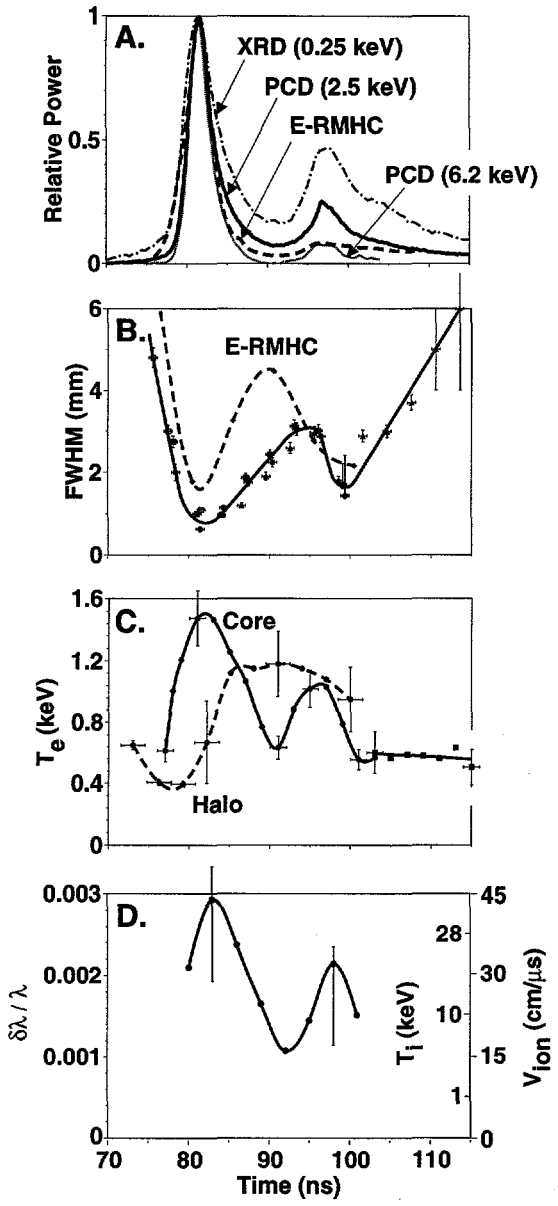

FIGURE 6. (A) Comparison of radiation pulses measured in XRDs and PCDs sensitive to x-rays in bands about 0.25, 2.5, and 6.2 keV with that simulated by the E-RMHC using reduced plasma emissivity for the 90-wire 8.6-mm radius Shot 2094.

(B) Comparison of the pinch diameter measured from fast-framing x-ray pinhole cameras (sensitive to x-rays greater than ~ 1 keV) with the E-RMHC mass-averaged radius associated with the Fig. 6A simulation, for three 90-wire, 8.6-mm radius Shots 2085, 2094, and 2095.

(C) Comparison of the core electron temperature for Shot 2094 with the average halo electron temperature for Shots 2085, 2094, and 2095.

(D) Opacity corrected Doppler broadened Lyman-beta transition for Shots 2085, 2094, and 2095.

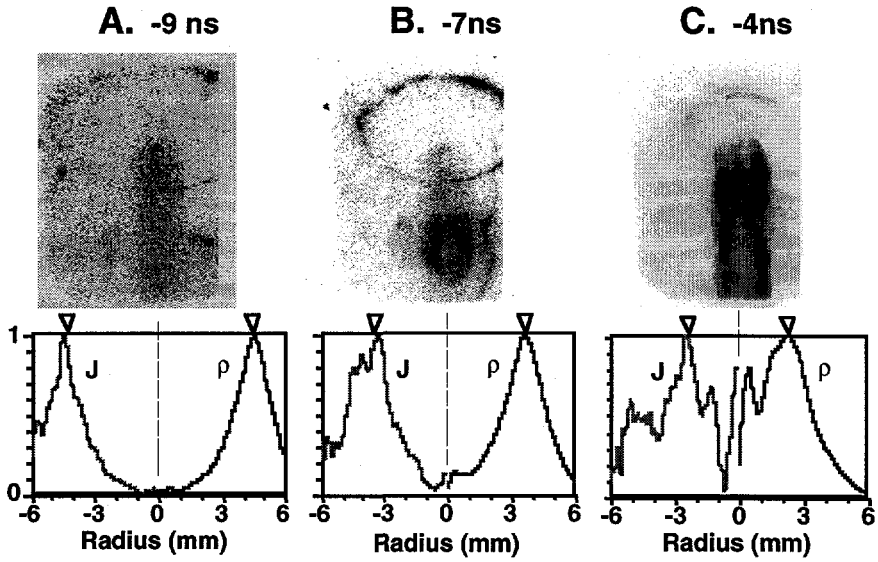

FIGURE 7. Comparison of fast-framing x-ray camera images (sensitive to 0.2 to 0.3 keV and greater than 1 keV x-rays) with E-RMHC simulations of mass and current density, –9, –7, and –4 ns before peak power for Shot 2235.

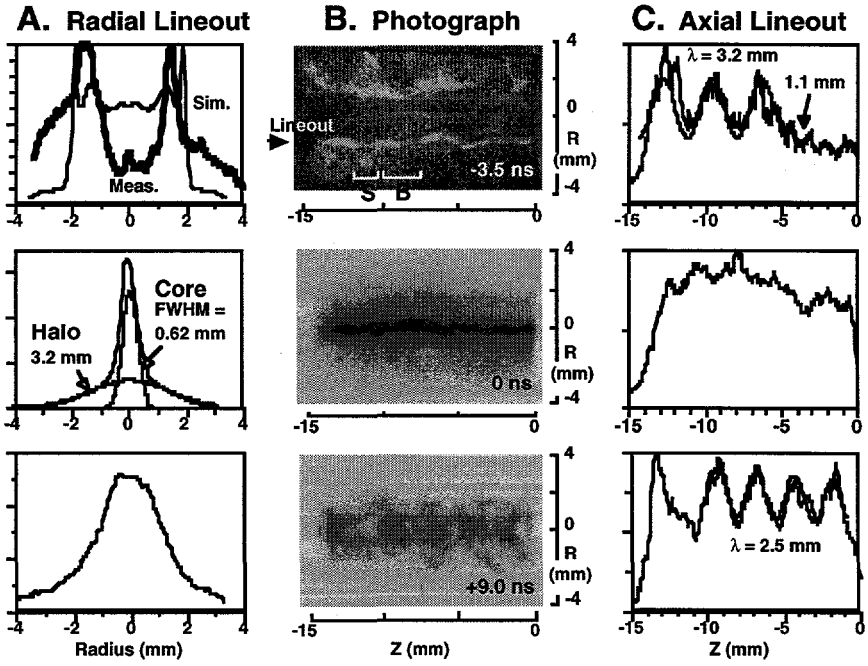

FIGURE 8. Comparison of fast-framing x-ray camera images and their associated lineouts –3.5, 0, and 9 ns with respect to the time of peak power. Images are sensitive to x-rays greater than 1 keV. The –3.5-ns image was also sensitive to 0.2 to 0.3 keV x rays.

In general, by adjusting a random density perturbation (8,10) given an initial plasma shell thickness, one can produce rz-RMHC simulations that replicate many of the features measured at the first implosion. This perturbed density seeds the growth of a magnetic Rayleigh-Taylor (RT) instability in the rz plane, which influences and limits the radial convergence. Owing to the use of a LTE approximation in the simulations and because of the 3D nature of the implosion which limits the compression, greater radiation cooling occurs in the simulation than is physical (9). The cooler plasma has reduced radial expansion following stagnation and the simulated plasma rapidly reaches a quasi-equilibrium without going through the second compression seen experimentally. A reduction in the plasma emissivity, as is done in some of the E-RMHC simulations, however, permits more realistic peak powers to be simulated and simultaneously generates a second convergence as shown in Figs. 6A and 6B.

Near peak emission, the radial lineouts of these images when integrated over the axial length of the pinch (Fig. 8A (0 ns)) are well fit by the sum of an intense Gaussian-like core surrounded by a diffuse Gaussian-like halo. Radially resolved images of the x-ray spectrum and temporally resolved x-ray spectra show that K-shell free-bound continuum emission originates from the core, whereas K-shell line emission originates from both the core and halo (17) in agreement with 1D-RMHC simulations (19). The time-resolved slope of the optically-thin free-bound emission measured with filtered photoconducting detectors (PCDs) gives a spatially average temperature of the electrons in the core (17), and the ratio of the time-resolved optically-thick hydrogen-like to helium-like line emissions gives a measure of the electron temperature in the halo (19) (Fig. 6C). The Doppler broadened line emission provides an estimate of a generalized ion temperature corresponding to a combination of line emission shifts caused by the coherent radial motion of the plasma, motion from fluid turbulence, micro instabilities, and intrinsic ion thermal motions (Fig. 6D) (9). The measured hot and then cooler core electron temperatures and ion temperatures/velocities correlate in time with the two radiation bursts and radial compressions, as expected for multiple implosions (Fig. 6). At peak convergence, the temperature of the halo ($\sim$ 0.4 keV) is estimated to be three to four times cooler than that of the core ($\sim$ 1.4 keV) (Fig. 6C), indicating the presence of strong temperature gradients. While both line and continuum emissions are generated in the hot plasma core at the time of peak convergence, only the optically-thin continuum x rays escape the plasma directly. The optically-thick line emission is absorbed and reemitted from the cooler regions until the pinch expands and the plasma opacity declines. The high temperatures inferred from the line analysis at times when the plasma is expanding and the core electrons are cooling (Fig. 6C), implies a lag in ionization. That is, the ionization state is no longer in equilibrium with the cooled electrons, but reflects instead the

earlier state of the plasma when the electrons were hot and the plasma was in equilibrium. The core electrons cool too rapidly in this case for recombination processes to maintain ionization equilibrium.

The early time characteristics of the plasma-shell implosions are illustrated in Fig. 7 and Fig. 8A (–3.5 ns). The rings evident in Fig. 7 are hypothesized to be from a radiating cathode plasma produced by the electron-current flow into the cathode from the surface of the imploding plasma shell (Fig. 1A). In support of this hypothesis, the radii of the rings correlate with both the mass-averaged and current-density averaged radii calculated by the E-RMHC simulation (Fig. 7). In the simulation, the calculated radially converging plasma precursor begins to stagnate on axis 9 ns prior to peak emission (Fig. 7A), reaching electron temperatures of ~ 1 keV. As expected and measured, this precursor becomes detectable just at this time. As the implosion evolves in the simulation, plasma accretes on axis, producing the appearance of a hot inward moving shell (Fig. 7C). The L-RMHC simulation of such a shell, which takes account of camera sensitivity and 35° viewing angle (Fig. 1A), is shown in Fig. 8A (–3.5 ns) for Shot 2085 (9).

These observations are also consistent with the 1D-RHMC analyses (19) that required a cool shell of plasma to implode onto a small amount of precursor plasma to explain the total to K-shell power ratio. In this model, the cool outer shell of plasma is needed to explain the greater than 4-to-1 power ratio, and it is also consistent with the spectral analysis (17,19) that found that only 20% of the mass contributing to K-shell radiation at the time of peak power. Moreover, the experimentally observed size of the K-shell emission region being smaller than the calculated plasma size (Figs. 6B and 7C) is consistent with this low-mass fraction contributing to the K-shell emission.

In Fig. 8A (–3 ns), the bubble and spike structure associated with the RT instability is seen. Axial lineouts of the image show the presence of 1-mm wavelengths that spatially merge with 3-mm wavelengths (Fig. 8C (–3.5 ns)). These wavelengths are characteristic of those simulated by the L-RMHC (9) and E-RMHC (1), respectively. As the pinch expands after stagnation, an m=0 sausage instability sets in (Fig. 8 (9 ns)). The correspondence between the periodicities measured prior to (Fig. 8C (–3 ns)) and after stagnation (Fig. 8C (9 ns)) suggests that the RT instability seeds the sausage instability. These observations are consistent with the rz-RMHC simulations.

Both rz-RMHC simulations show that the main radiation pulse begins when the main RT bubble reaches the axis and ends when the spike finishes stagnating on axis. This 2D feature is consistent with: (1) the measured width of the radiation pulse (~ 5 ns, Fig. 6A), (2) the few mm thickness of the plasma inferred just prior to stagnation from either the image of Fig. 7C or the radial length of the

spikes in Fig. 8B (– 3.5 ns), (3) and the implosion velocity of ~ 0.5 mm/ns inferred from time-resolved implosion images (9).

MASS AND RADIUS VARIATION

The variation in the widths of the total radiation pulse that was measured in the mass and radius experimental sequence is well described by E-RMHC simulations in which the magnitude of the random density perturbations (15,16) is kept constant. Two theoretical curves are shown in Figs. 9A, 9B, 10A, and 10B. The dashed curve corresponds to the use of the nominal plasma emissivity (10). The solid curve corresponds to a reduced emissivity, in an attempt to reproduce the second peak in the radiation pulse (Fig. 6A) and the measured power levels at ~ 0.6 mg load mass (Fig. 9B). Differences between the two curves provide an estimate of the uncertainty introduced by the approximation used for the Planckian emission-absorption opacity in the E-RMHC. As shown in Figs. 9B and 10B, the measured peak power is bracketed by either calculation, which, together with the agreement in pulse width, provides credibility to the average hydrodynamics of the E-RMHC simulations.

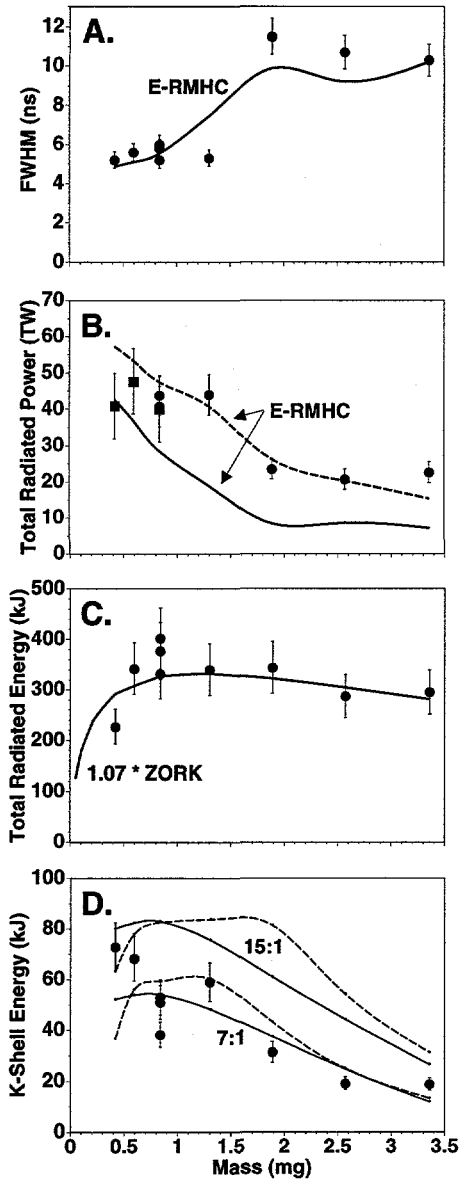

FIGURE 9. (A) Comparison of measured and E-RMHC calculated total-radiated power pulse width.

(B) Comparison of measured (uncorrected) and E-RMHC calculated total radiated power. ■ corresponds to loads with less than 192 wires corrected for gap effect (Fig. 4).

(C) Comparison of measured total radiated energy (uncorrected) versus scaled (1.07±0.14) ZORK calculation using measured radial convergence of 20-to-1.

(D) Comparison of measured K-shell yield versus that simulated by the Mosher two-level model (solid curve) and the Whitney-Giuliani scaling model (dashed curve) versus array mass for 7:1 and 15:1 radial convergences.

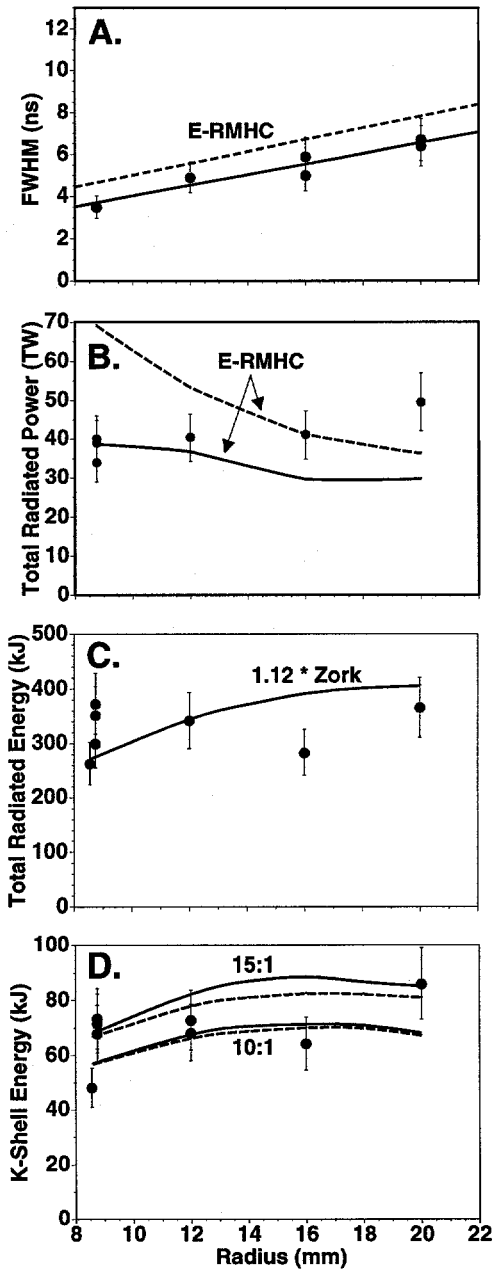

FIGURE 10. (A) Comparison of estimated (measured using XRD filtered by 5 μm Kimfol) and E-RMHC calculated total radiated power pulse width.
(B) Comparison of measured (uncorrected) and E-RMHC calculated total radiated power.
(C) Comparison of measured total radiated energy (uncorrected) versus scaled (1.12±0.28) ZORK calculation using measured radial convergence of 19:1 to 37:1 as radius increased from 8.6 to 20 mm, respectively.
(D) Comparison of measured K-shell yield versus that simulated by the Mosher two-level model (solid curves) and the Whitney-Giuliani scaling model (dashed curves)versus array radius for 10:1 and 15:1 radial convergences.

Therefore, about 60% of the total radiated energy (corrected) can be accounted for by the kinetic energy (corrected) delivered to the load. The remaining 40% is likely due to additional pdV work and the slight Joule heating given the load and is approximately consistent with that calculated by L-RMHC for Shot 2094 (9).

The Mosher-Qi-Krishnan two-level (15) (solid curves in Figs. 9D and 10D) and the 1D Whitney-Giuliani (20) scaling (dashed curves in Figs. 9D and 10D) model yields are in qualitative agreement with that measured (Figs. 9D and 10D), using ZORK kinetic energies derived from convergence ratios varying between 7 and 15 with the full imploded mass. These models depend only on the kinetic energy delivered to the load, the peak radial convergence, and participating mass, and they ignore the multi-dimensional dynamics of the implosion and plasma radiation after stagnation. The predicted variation with mass is due to the change in both temperature and density for the nearly-fixed kinetic energy (Fig. 9C). The predicted variation in yield with radius is due primarily to the slight variation in the kinetic energy (Fig. 10C). The constancy of yield with radius reflects the optically thick nature of the emission for aluminum.

SUMMARY

Increasing the wire number has produced significant improvements in pinch quality, reproducibility, and x-ray output power. The mass variation experimental series, which was done for high-wire-number plasma-shell loads, shows that a factor of two decrease in pulse width and an associated doubling of the radiated x-ray power and a greater-than-two increase in K-shell yield occurs when the load mass transitions from masses greater than 1.9 mg to those less than 1.3 mg, in qualitative agreement with the E-RMHC and simple K-shell models. In the high-power, low-mass, plasma-shell regime, the peak power and K-shell yields remain relatively flat with increased radius, again in agreement with the E-RMHC and the K-shell models. Importantly, the high quality of the implosions generated by the large-radii loads gave us confidence in using such high-wire-number, plasma-shell loads for PBFA-Z. The large radius enabled the initial electral stress on PBFA due to load inductance to be kept to a minimum, as the power flow in the upstream portion of the accelerator was improved. In conclusion, these experiments have conclusively demonstrated the necessity of using a large number of wires within a wire array in order to optimize the x-ray energy and power output from z-pinch implosions, and they represent a breakthrough in z-pinch implosion load configurations for large pulsed power generators (4).

ACKNOWLEDGMENTS

We thank T. L. Gilliland, D. O. Jobe, J. S. McGurn, P. E. Pulsifer (NRL), J. F. Seamen, K. W. Struve, W. A. Stygar, J. W. Thornhill (NRL), and M. F. Vargas for their dedicated technical support; G. O. Allshouse, A. Toor (LLNL), M. Tabak (LLNL), and C. Deeney for useful discussions; M. K. Matzen, J. E. Maenchen, and D. H. McDaniel, M. E. Jones (LANL), A. Toor (LLNL), and J. Davis (NRL) for vigorous programmatic support; M. K. Matzen for carefully reviewing and L. O. Peterson for typing this manuscript. Sandia is a multiprogram laboratory operated by Sandia Corporation, a Lockheed Martin Company, for the United States Department of Energy under Contract DE-ACO4-94AL85000.

REFERENCES

1. Sanford, T. W. L., Allshouse, G. O., Marder, B. M., Nash, T. J., Mock, R. C., Spielman, R. B., Seamen, J. F., McGurn, J. S., Jobe, D., Gilliland, T. L., Vargas, M., Struve, K. W., Stygar, W. A., Douglas, M. R., Matzen, M. K., Hammer, J. H., De Groot, J. S., Eddleman, J. L., Peterson, D. L., Mosher, D., Whitney, K. G., Thornhill, J. W., Pulsifer, P. E., and Apruzese, J. P., *Phys. Rev. Lett.* 77,5063 (1996).
2. Bloomquist, D. D., Stinnett, R. M., McDaniel D. H., Lee, J. R., Sharpe, A. W., Halbleib, J. A., Shlitt, L. G., Spence, P. W., and Corcoran, P., *Proc. 6th Int. IEEE Pulsed Power Conf.*, Arlington, VA, ed. P. J. Turchi and B. H. Bernstein (IEEE, New York, 1987), p. 310.
3. Deeney, C., Nash, T. J., Spielman, R. B., Seamen, J. F., Chandler, G. Struve, K. W., Porter, J. L., Stygar, W. A., McGurn, J. S. Jobe, D. O., Gilliland, T. L., Torres, J. A., Vargas, M. F., Ruggles, L. E., Breeze, S., Mock, R. C., Douglas, M. R., Fehl, D., McDaniel, D. H., and Matzen, M. K., "Power Enhancement by Increasing Initial Array Radius and Wire Number of Tungsten Z Pinches," submitted to *Phys. Rev. E* (1996).
4. Matzen, M. Keith, "Z Pinches as an Intense X-ray Source for High-Energy Density Physics Applications," to be published *Phys. Plasmas* (1997).
5. Pereira, N. R. and Davis, J., *J. Appl. Phys.* **64**, R1 (1988).
6. Spielman, R. B., De Groot, J. S., Nash, T. J., McGurn, J., Ruggles, L., Vargas, M., and Estabrook, K. G., *Dense z-Pinches*, presented at the 3rd International Conference, London, UK, 1993, AIP Conference Proceedings 299, editors H. Haines and A. Knight, American Institute of Physics, New York 1994, L.C. Catalog Card No. 93-74569, pages 404-420.
7. Deeney, C., Nash, T. J., Spielman, R. B., Seaman, J. F., Douglas, M. R., McGurn, J. S., Jobe, D. O., Gilliland, T. L., Mock, R. C., Struve, K. W., Whitney, K. G., Pulsifer, P. E., Apruzese, J. P., and Thornhill, J. W, "Improved Large Diameter Wire Array Implosions from Increased Wire Array Symmetry and On-axis Mass Participation", to be submitted to *Phys. Plasmas* (1997).
8. Hammer, J. H., Eddleman, J. L., Springer, P. T., Tabak, M., Toor, A., Wong, K. L., Zimmerman, G. B., Deeney, C., Humphreys, R., Nash, T. J., Sanford, T. W. L., Spielman, R. B., and De Groot, J. S., *Phys. Plasmas* **3**, 2063 (1996).
9. Sanford, T. W. L., Nash, T. J., Mock, R. C., Spielman, R. B., Struve, K. W., Hammer, J. H., De Groot, J. S., Whitney, K. G., and Apruzese, J. P., to be published *Phys. Plasmas* **4**, (1997).
10. Peterson, D. L., et al., *Phys. Plasmas* **3**, 368 (1996).
11. Matuska, W., et al., *Phys. Plasmas* **3**, 1415 (1996).
12. Thornhill, J. W., Whitney, K. G., and Davis, J., *J. Quant. Spectrosc. Radiat. Transfer* **44**, 251 (1990).
13. Spielman, R. B., et al, Paper O-4-3 in *Proceedings of the 10th International Conference on High-Power Particle Beams*, Prague, Czech Republic, June 10-14, 1996, ed. K. Jungwirth and J. Ullschmied, pages 150 to 153. Copies of the conference proceedings can be ordered

from BEAMS96, Institute of Plasma Physics, Czech Academy of Sciences, Za Slovankou 3, 182 00 Prague, Czech Republic.
14. Spielman, R. B., et al., ***Bull. Am. Phys. Soc.*** **41**, 1422 (1996).
15. Sanford, T. W. L., Peterson, D. L., Roderick, N. F., Mosher, D., et al., "Increased X-ray Power Generated from Low-Mass Larger-Number Aluminum-Wire-Array Z-Pinch Implosions," to be submitted to *Phys. Plasmas* (1997).
16. Sanford, T. W. L., Peterson, D. L., Roderick, N. F., Mosher, D., et al. "Symmetric Aluminum-Wire Arrays Generate High-Quality z-Pinches at Large Array Diameters", to be submitted to *Phys. Plasmas* (1997).
17. Sanford, T. W. L., Whitney, K. G., Nash, T. J., Mock, R. C., Apruzese, J. P., Gilliland, T. L., Jobe, D. O., McGurn, J. S., Pulsifer, P. E., Seamen, J. F., Spielman, R. B., Thornhill, J. W., and Vargas, M. F., *Rev. Sci. Instrum.*, 68, 852 (1997).
18. Sanford, T. W. L., Humphreys, D. R., Poukey, J. W., Marder, B. M., Halbleib, J. A., Crow, J. T., Spielman, R. B., and Mock, R. C., Sandia National Laboratories Technical Report SAND94-0694 (June 1994).
19. Whitney, K. G., Thorhill, J. W., Pulsifer, P. E., Apruzese, J. P., Sanford, T. W. L., Nash, T. J., Mock, R. C., and Spielman, R. B., submitted to *Phys. Rev. E* (1996).
20. Whitney, K. G., et al., *J. Appl. Phys.* **67**, 1725 (1990).